Using computer simulations to study the effect of laminin and fibronectin on a biomechanical model of solid tumour growth

Catherine Hastings

Abstract

We seek to find out more about the effects of including proteins laminin and fibronectin into a continuum model of tumour growth. We first outline the basics of cancer biology, and give a brief explanation of how solid tumour growth can be modelled mathematically. We give a description of 3D *in vitro* experiments being carried out alongside this work. The equations describing our model are listed, along with some of the variations that can be made. We have found our model effectively incorporates these peritumoural proteins, and that the determination of parameters is as important to the output of the model as changes in the variable protein concentration.

1 Introduction

1.1 Cancer Biology

Cancer is the name for the disease that occurs when mutations in genes accumulate to the extent that affected cells no longer respond to signals controlling the normal cell cycle, and accordingly grow, divide and spread. Cancer cells invade the surrounding healthy tissue, and in late stages spread to further parts of the body (Cooper and Hausman, 2000).

A tumour is the name for a group of cancerous cells. The tumour is defined to be solid if the collection of cancerous cells is stiffer than the surrounding tissue Nyga et al. (2011). This surrounding tissue is called the peritumoural stroma. It is a modified form of the extracellular matrix (ECM), the noncellular component present in all tissues. The ECM is composed of water, proteins and polysaccarides, but varies significantly in its exact make-up, depending upon the type of tissue and many other factors (such as age and pathology). The function of the ECM is to provide physical support to surrounding cells, but also to act as a key part of biochemical and biomechanical cell interaction (Frantz et al., 2010).

There are two types of protein in the ECM, proteoglycans and fibrous glycoproteins. The proteoglycans are smaller molecules which form a hydrated gel. The fibrous proteins, such as collagen, laminin and fibronectin are longer molecules which sit within this gel.

Laminin is a key component of the basement membrane, which is the thin matrix of proteins between epithelial cells and the extracellular matrix, whereas fibronectin is largely found in ECM itself (Engel et al., 1981). In healthy tissue, it has been shown that laminin, along with collagen type IV, is involved in cellular adhesion to the basement membrane and to the ECM. Fibronectin is also involved with cell-matrix adhesion, but also cell-cell adhesion, cell migration, morphogenesis and differentiation. In tissue surrounding cancerous tumours it has been shown that both laminin and fibronectin play a role in regulating cell migration, facilitating tumour invasion (Ioachim et al., 2002).

It can therefore be concluded that the composition of the peritumoural stroma has a significant impact on tumour growth. In particular there are known mechanisms by which an increased concentration of the glycoproteins laminin and fibronectin can promote tumour growth.

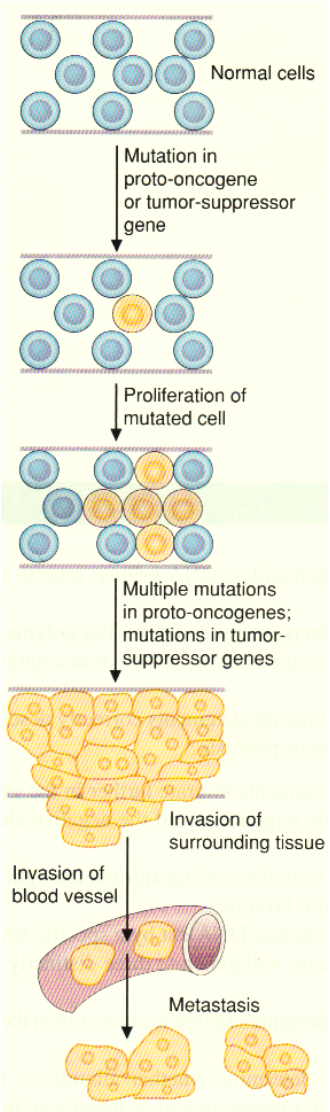

Figure 1.1: Diagram showing the progression of cancer, from first mutation to metastasis. From Lieberman et al. (2009).

1.2 Experimental procedure

This work is more particularly motivated by laboratory work, which aims to mimic tumour growth by building 3D scaffolds for small

tumouroids, and monitoring the shape and rate of the outgrowth of cancer cells over time.

This interplay between experimental work and mathematical modelling hopes that computer simulations will provide a deeper understanding of the most important elements in tumour growth, and give an idea which are the most valuable experiments to perform. This is particularly important given that these experiments are very time consuming, typically lasting between 7 and 21 days. Equally, laboratory work provides a strong physical basis of evidence upon which to ground the simulations.

The 3D scaffolds are made by using a technique similar to that described by Nyga et al. (2013). Two cell lines of human osteosarcoma are cultured, one line more agressive and more likely to metastasise than the other. A small disc of cancer cells is then translated on to a collagen-based hydrogel, containing various concentrations of laminin and fibronectin. A further layer of hydrogel is placed over the cancer cells, and the entire structure is plastically compressed, in order to make the experiment as biomimetic as possible.

The result is a small disc (approximately 7mm in width) of cancer cells surrounded on all sides by hydrogel, resulting in a larger disc of approximately 20mm. The disc is only 100µm thick. However, this is still sufficiently thick to mimic the conditions in human tissue.

The tumouroids are monitored daily, and left to grow for 7 days. The cells are then fixed and the results are collected using light microscopy (see figure 1.2). The amount of tumour outgrowth is quantified, and the results can be analysed statistically.

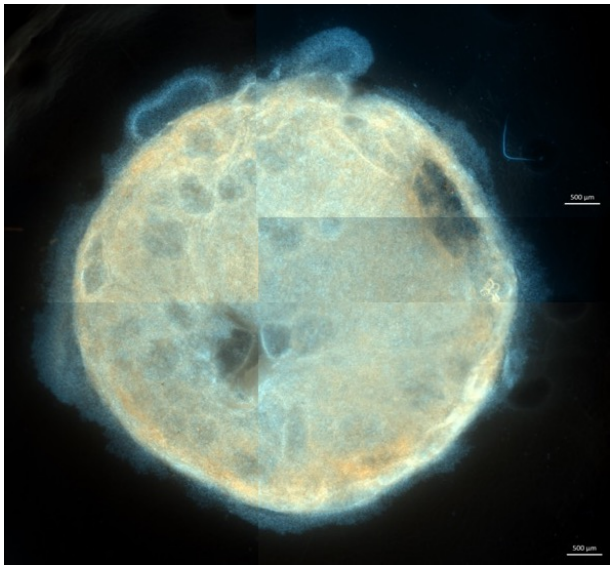

Figure 1.2: A photograph from light microscope showing typical results of a tumouroid grown in a 3D *in vitro* scaffold.

Preliminary experiments have been carried out. The collagen-based hydrogel was mixed with either: $0.25\,\mu g\,ml^{-1}$ of laminin or fibronectin, $0.50\,\mu g\,ml^{-1}$ of laminin or fibronectin, or $0.25\,\mu g\,ml^{-1}$ of laminin and $0.25\,\mu g\,ml^{-1}$ of fibronectin. Some results are shown in figure 1.3.

The error bars here show the standard error for each sample (i.e. the standard deviation for each sample divided by the square root of the sample size). However, the standard deviations for each sample are much higher. [The largest standard deviation out of any of the samples is 276 from a mean of 417. This is for the sample with $0.25\,\mu g\,ml^{-1}$ each of fibronectin and laminin.]

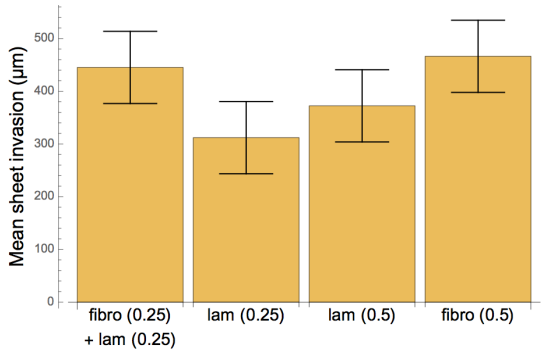

(a) An aggressive osteosarcoma cell line.

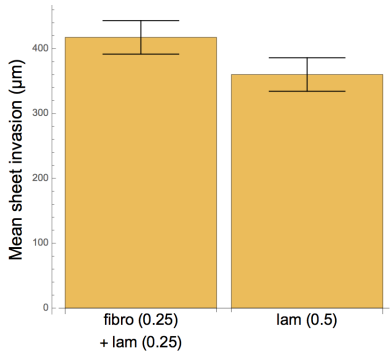

(b) A less aggressive osteosarcoma cell line.

Figure 1.3: Bar charts showing the average distance of tumour outgrowth for different concentration of proteins in the ECM surrounding an artificial cancer mass.

This highlights that there is wide variation within each sample. Therefore, the results of this data cannot be relied upon too heavily.

1.3 Modelling tumours

There are many ways of mathematically modelling tumour growth. The first decision to be made is upon which physical phenomena to base the model. For example, models have been created based upon reaction-diffusion equations for the nutrients required for tumour growth. But it should be noted that cells respond to the stiffness of the surrounding material (Discher et al., 2005). More specifically, it has been shown that increasing stiffness of the peritumoural stroma results in reduced tumour outgrowth (Helmlinger et al., 1997). Therefore, for this work, a biomechanical approach shall be taken, focussing of the physical properties of the tumour and its surrounding tissue.

The are mechanisms which affect tumour growth on many different scales: from the molecular level, through the cell scale and finally at the macro-scale of tissues. All of these different scales can be included in a mathematical model, and combinations of different scales can also be considered (such as in Wijeratne et al. (2015)). Here the focus is on the macro-scale, with the tumour and the peritumoural stroma modelled as a two-compartment continuum.

Human tissue is not solid, but a heterogeneous combination of solids and fluids. This can be taken into account in a model by, for example, modelling the tumour as poro-elastic (i.e a sponge-like solid) filled with liquid. Tumours also promote the formation of blood vessels in their surrounding tissue in order to ensure a lasting supply of nutrients. The vascular nature of a tumour can be included in a mathematical model. Many of these extra considerations, and how to model them, are described in detail by Cristini and Lowengrub (2010).

For this work we implement a single phase, avascular continuum model. This means that the numerical solution is relatively simple to implement, and results can be produced quickly.

2 Method

The tumour is modelled as a continuum with two compartments, a solid tumour compartment, Ω_{T}, surrounded by the peritumoural stroma, Ω_{S}. The model is defined in terms of the biomechanical properties of the tumour. The variable being solved for is $\mathbf{U}$, the solid displacement vector. The system obeys the principle of conservation of mass, and so accordingly

$$\nabla \cdot \mathbf{V} - Q = 0 \ ,$$

where $\mathbf{V} = \frac{\mathrm{d}\mathbf{U}}{\mathrm{d}t}$ is the solid velocity and Q represents body forces and source terms. Here, ∇ is defined to be equivalent to $\frac{\partial}{\partial \mathbf{X}}$ where $\mathbf{X}$ is the space vector in the Lagrangian frame of reference. Linear momentum is also conserved and so

$$\nabla \cdot \mathbf{S} - \mathbf{Q} = 0 \ ,$$

where $\mathbf{S}$ is the 2nd Piola-Kirchoff stress tensor and $\mathbf{Q}$ represents body forces and source terms.

In order to determine the stress tensor $\mathbf{S}$, the tumour and stroma can be modelled as a hyperelastic material and laws from continuum solid mechanics (Holzapfel, 2000) can be applied to define a constitutive law. It should first be noted that the deformation gradient tensor $\mathbf{F}$ can be decomposed into its elastic and growth parts, giving

$$\mathbf{F} = \mathbf{F}_{\mathrm{e}} \cdot \mathbf{F}_{\mathrm{g}} \ .$$

This deformation gradient is defined with respect to the initial configuration, $\mathbf{F} = \mathbf{I} + \frac{\partial \mathbf{U}}{\partial \mathbf{X}}$. The stretching part of the deformation gradient is symmetric and defines the right Cauchy-Green tensor $\mathbf{C} = \mathbf{F}_{\mathrm{e}}^{\mathrm{T}}\mathbf{F}_{\mathrm{e}}$. $\mathbf{C}$ is also symmetric and therefore has invariants, one of which is $I_1 = \mathrm{tr}\,(\mathbf{C})$. Using these, Voutouri et al. (2014) have defined a constitutive law for hyperelastic solids, which defines the strain-energy function to be

$$\Psi = \frac{\mu}{2}\left(I_1 - 3\right) + \frac{K}{2}\left(J - 1\right)^2 \ , \qquad (1)$$

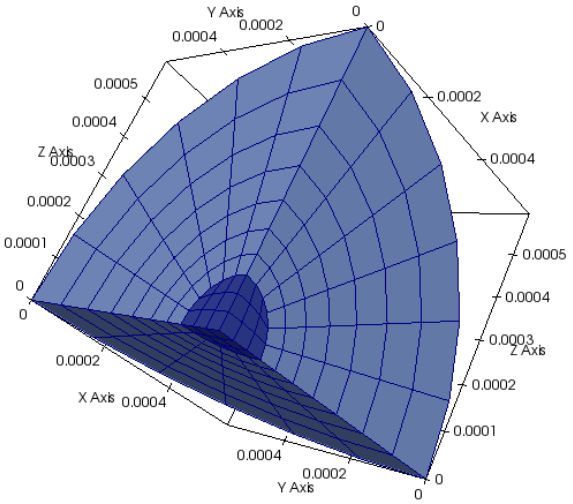

Figure 2.1: A representation of the tumour and its surrounding stroma, with the mesh for the finite element analysis also depicted. The unit of length along the axes is metres.

where μ and K correspond to the shear and bulk moduli respectively and $J = \det\left(\mathbf{F}_{\mathrm{e}}\right)$. The 2nd Piola-Kirchoff stress tensor can then be obtained from the relation

$$\mathbf{S} = 2\frac{\partial \mathbf{\Psi}\left(\mathbf{C}\right)}{\partial \mathbf{C}} \ .$$

The growth-induced displacement in Ω_{T} is prescribed by the expression for tumour growth

$$\mathbf{F}_{\mathrm{g}} = f\left(C\right)\mathbf{I} \ , \qquad (2)$$

where $f(C)$ can be any smooth function based upon substrate concentrations C. This growth function is only implemented in the tumour compartment. However, this growth in turn affects the displacement in the peritumoural stroma, Ω_{S}.

The model is implemented in an octant of a sphere (as depicted in figure 2.1), in order to reduce computation time. The radius of the sphere is 0.6mm, and the tumour radius starts at 0.1mm. Due to the fact that only an octant is being modelled, there are three additional flat surfaces that need to be taken into account. These surfaces are labelled Γ^{S} due to their presence being due to the assumption of spherical symmetry.

The equations defining the model are subject to the initial condition $\mathbf{U} = 0$ when $t = 0$, and the boundary conditions

$$\begin{aligned} \mathbf{U} \cdot \mathbf{n} &= 0 \quad \text{for } \mathbf{X} \in \Gamma^{\mathrm{S}} \ , \\ \mathbf{S} \cdot \mathbf{n} &= 0 \quad \text{for } \mathbf{X} \in \Gamma^{\mathrm{I,E}} \ . \end{aligned}$$

Here Γ^{I} is the interface boundary between the tumour and the peritumoural stroma and Γ^{E} is the external boundary. $\mathbf{n}$ is the outward facing unit normal on a given surface.

Software implementing a 3D finite element method called FEB3 (Vavourakis and Wijeratne, 2016) was used to solve these equations. Either an implicit or explicit numerical method was implemented, namely either the Navier-Cauchy method or the forward Euler method respectively. The results were outputted so as to be easily processed by the visualisation software Paraview (Ayachit et al., 2015). The data was then manipulated and outputted as '.csv' files, and fed into Mathematica for further processing.

2.1 Parametric analysis

The model described above was implemented in order to perform a simple parametric analysis. Referring back to equation (2), the growth function first used was a Gompertz style growth law (Laird, 1964), with the amplitude determined by the equation

$$\frac{G_1 \, C_{\mathrm{O}}}{G_2 + C_{\mathrm{O}}} \ , \tag{3}$$

where C_{O} is the concentration of oxygen measured in mol m^{-3} and G_1 and G_2 are growth parameters with units of days^{-1} and mol m^{-3} respectively. This growth equation is based upon the Michaelis-Menton theory of reaction kinetics (Britton, 2003). For this section, the explicit numerical method was implemented.

The first parameters to be varied were the stiffness parameters K_{S} and μ_{S} in the peritumoural stroma, as described in equation (1). In general, the tumour is significantly stiffer than the material around it. The values implemented are listed in table 2.1. The values for the tumour

Sym.	Parameter Name	Tumour	Stroma	Units
μ	Shear modulus	725	710	Pa
K	Bulk modulus	14010	3080	Pa

Table 2.1: The original model parameter values used when varying the stiffness of the peritumoural stroma.

are to be kept constant throughout, while the stiffness parameters for the peritumoural stroma are to be reduced to 75% and 50% of the original values.

The second stage was to vary the value of the parameter G_1. Both G_1 and G_2 must be obtained experimentally as described by Casciari et al. (1992a), and the values used are motivated by Casciari et al. (1992b). The original values used are given in table A.1, and the variations are depicted along with the results in figure 3.4.

2.2 Including laminin and fibronectin

When adding the effect of laminin and fibronectin into the model there are three key considerations,

1. What form should the growth function $f(C)$ take, as described in equation (2)?
2. If using a form of $f(C)$ similar to that described in equation (3), based upon Michaelis-Menten reaction kinetics, what values of $G_{1,\mathrm{P}}$ and $G_{2,\mathrm{P}}$ should be used? (The subscript P represents that these parameters correspond to the effect of stromal proteins.)
3. How should we define the protein concentration C_{P}, given that experimentally the proteins are only present in the peritumoural stroma?

It could also be suggested that including the proteins laminin and fibronectin into the peritumoural stroma might have an effect on its stiffness, and that this should be reflected in the choices of the parameters for the shear and bulk moduli μ_{S} and K_{S}. However, according to (Deister et al., 2007; Marquardt and Willits, 2011), including these proteins does not significantly affect the physical attributes of the stroma. The values of μ and K shall be kept constant and the same as those used in section 2.1.

Using Casciari et al. (1992a) as a model, the growth function was redefined as

$$f(C) = \frac{G_{1,\mathrm{O}}\, C_{\mathrm{O}}}{G_{2,\mathrm{O}} + C_{\mathrm{O}}} + \frac{G_{1,\mathrm{P}}\, C_{\mathrm{P}}}{G_{1,\mathrm{P}} + C_{\mathrm{P}}} \ . \tag{4}$$

Similar to equation (3), this growth function relies upon Michelis-Menton reaction kinetics. For this section, the implicit numerical method was implemented.

$G_{1,\mathrm{P}}$ and $G_{2,\mathrm{P}}$ can be found experimentally. Values for G_1 and G_2 were obtained experimentally for oxygen and glucose by Casciari et al. (1992b) and Kim et al. (2011). Using their work as a model, the values for $G_{1,\mathrm{O}}$ and $G_{2,\mathrm{O}}$ used in section 2.1, were 2.8 days^{-1} and $7.3 \times 10^{-3}\,\mathrm{mol\,m}^{-3}$ respectively. Combining these facts, sensible values were estimated and the impact of changing protein concentrations upon computer simulations was studied.

Our preliminary data tests protein concentrations of 0.25 and $0.50\,\mu\mathrm{g\,ml}^{-1}$. Assuming a molecular weight of 440kDa for laminin and fibronectin, converting the units gives values of 5.68×10^{-4} and $1.13 \times 10^{-3}\,\mathrm{mol\,m}^{-3}$ respectively. Accordingly, for $G_{2,\mathrm{P}}$, an estimate of $5.65 \times 10^{-5}\,\mathrm{mol\,m}^{-3}$ was chosen. It should be noted that 5.65×10^{-5} is 5% of 1.13×10^{-3} and 10% of 5.68×10^{-4}. The values of G_1 implemented were $G_{1,\mathrm{O}} = G_{1,\mathrm{P}} = 1.4$. The full table of parameters is given in table A.3.

Experimentally, the proteins laminin and fibronectin are only included in the stroma. To reflect this in the model, the concentration of laminin was defined to be

$$C_{\mathrm{P}} = \begin{cases} 0.0 & \text{for } 0 \leq r < 0.09 \ , \\ c & \text{for } 0.09 \leq r \leq 0.6 \ , \end{cases}$$

where r is the radius measured in mm. Simulations were run with c taking values of 2.26×10^{-3}, 5.68×10^{-4} and 1.41×10^{-4} mol m^{-3}.

There is an argument to be made that the laminin and fibronectin might not be uniformly spread through the stroma. In healthy human tissue the extracellular matrix is very heterogeneous (Frantz et al., 2010), and in laboratory experiments the stromal proteins are combined with the collagen gel with manual mixing. Therefore introducing some heterogeneity into the distribution of the proteins might be appropriate. Therefore, two alternative models were implemented, the first being

$$C_{\mathrm{P}} = \begin{cases} \alpha\, r & \text{for } 0 \leq r < 0.09 \ , \\ \beta - \gamma\, r & \text{for } 0.09 \leq r \leq 0.6 \ , \end{cases}$$

again, with the radius r being measured in mm. α, β and γ are positive constants chosen so that a maximum concentration of 5.65×10^{-5} mol m^{-3} occurred at $r = 0.09$, that $0.09\alpha = \beta - 0.09\gamma$ and that $\beta - 0.6\gamma = 0$.

The second model defines the protein concentration to be dependent on the angles θ and φ, as used to describe standard spherical coordinates, i.e. where

$$\begin{aligned} x &= r\, \sin\varphi\, \cos\theta \ , \\ y &= r\, \sin\varphi\, \sin\theta \ , \\ z &= r\, \cos\varphi \ , \end{aligned}$$

with $r \in [0, 0.6]$, $\theta \in \left[0, \frac{\pi}{2}\right)$ and $\varphi \in \left[0, \frac{\pi}{2}\right]$. The concentration was then defined as

$$C_{\mathrm{P}} = a \left(\frac{\pi^2}{4} - 4 \left(\varphi - \frac{\pi}{4} \right)^2 + \frac{\pi^2}{16} - \left(\theta - \frac{\pi}{4} \right)^2 \right) \ ,$$

with a chosen so that the maximum concentration, when $\theta = \varphi = \frac{\pi}{4}$, was $C_{\mathrm{P}} = 5.68 \times 10^{-4}$ mol m^{-3}. When varying the function determining the concentration of stromal protein, special effort was made to ensure that the maximum concentration implemented was the same for each function.

3 Results

3.1 Parametric analysis

For each set of simulations run in this section, there are three possible plots: displacement against radius, displacement against time and stress against time.

It should be noted that the displacement is always positive, and can be interpreted as a direct measure of how much the tumour has grown. Similarly, a correspondence can be made between the slope of a displacement-time graph and the rate at which the tumour is growing. Each figure plotting the displacement against the radius, shows the displacement at the time point $t = 25$ days. By comparing this with a figure plotting displacement against time, it can be seen that $t = 25$ days, is the time of maximum displacement.

Figure 3.2 shows the effect of varying the stiffness of the peritumoural on the displacement of the mesh from its original position. The plots show that reducing the stiffness of the peritumoural stroma both slightly increases the rate of growth and the amount maximum amount

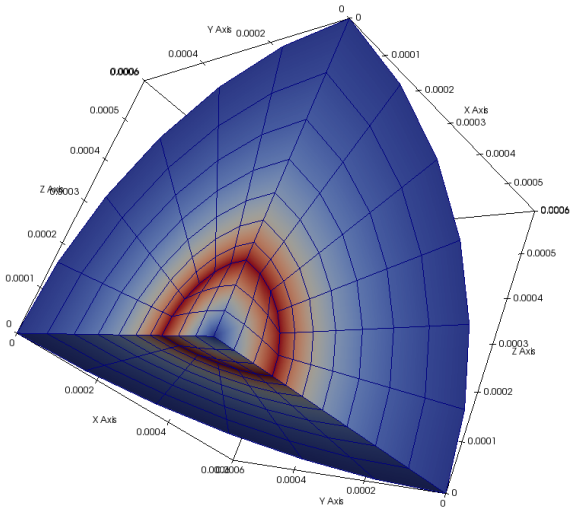

Figure 3.1: A representation of what the tumour looks like after a simulation has been run. The increase in red represents areas experiencing large displacement. The mesh has been warped to according to this displacement.

that a tumour grows in a given period of time. Figure 3.2a shows that the point of maximum displacement occurs at $r = 0.1$mm which corresponds to the tumour boundary. It can also be seen that the displacement increases sharply and linearly with radius, up to $r = 0.1$mm. After the tumour boundary the amount of displacement decreases non-linearly, with the outer boundary $r = 0.6$mm experiencing no displacement.

Studying the shape of graph 3.2b shows that the tumour grows slowly at first, and that the rate of growth increases with time. This is due to the Gompertz growth law that was implemented, being that Gompertz-type growth is an exponential function.

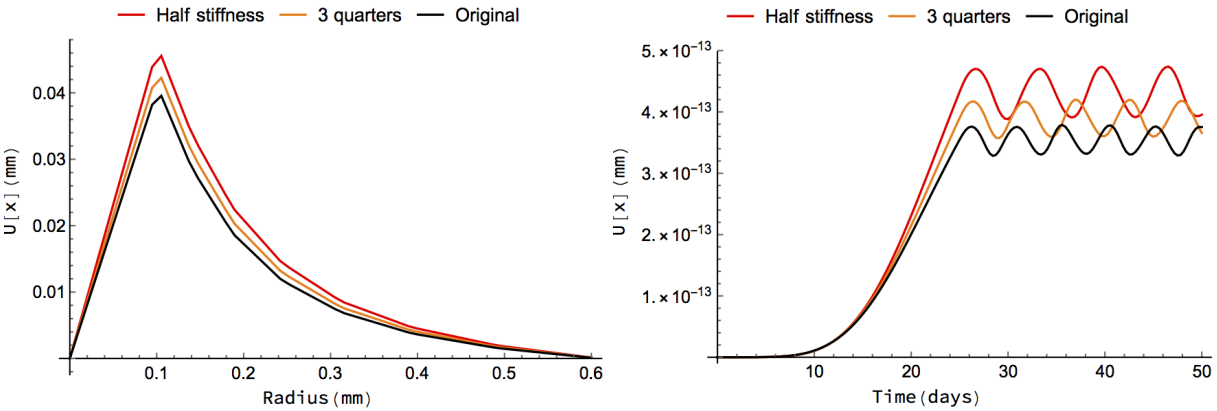

(a) Displacement against radius at 25 days.

(b) Space-averaged displacement against time.

Figure 3.2: Plots showing how the displacement changes over the radius and over time, when we vary the stiffness parameters K_S and μ_S (Pa).

One of the benefits of using a model based upon the biomechanics of tumour growth, is that it allows very easily for the calculation of the stress that a tissue undergoes. Figure 3.3 shows that both the tumour cells and the surrounding stroma undergo an increase in the stress exerted on them. The plot also shows that this effect is reduced as the peritumoural stroma reduces in

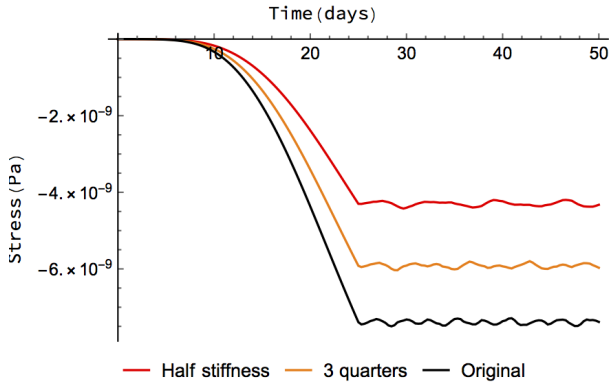

Figure 3.3: Plot showing how the space-averaged stress varies over time when we vary the stiffness parameters K_S and μ_S (Pa).

stiffness.

Comparing plots 3.2b and 3.3 shows that whilst decreasing the stiffness of the stroma has the effect of a relatively small percentage increase on the displacement of the tumour cells, the average stress felt by the tissue is significantly decreased.

Looking at the results from varying the parameter G1 in figure 3.4, it can be deduced that increasing the value of G1, increases the rate of tumour growth and the total amount of displacement felt by the tumour cells. This effect appears to be almost linear. By this it is meant that, in increasing the value of G1 by a factor of 1.4 from 2.8 to 4 days^{-1}, the displacement increases by a factor of 1.25, from 0.04 to 0.05mm.

It can also be noted that increasing the value of G1 has a much more pronounced effect on the rate of tumour growth than decreasing the peritumoural stiffness. Comparing the slopes of figures 3.2b and 3.4b, a decrease by factor 2 in the stiffness has a very small impact on the rate of growth, whilst increasing G1 by a factor of 1.4 has a larger impact on the rate of growth.

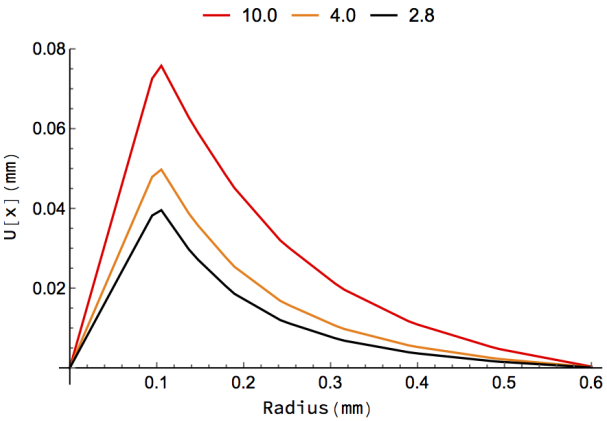

(a) Displacement against radius at 25 days.

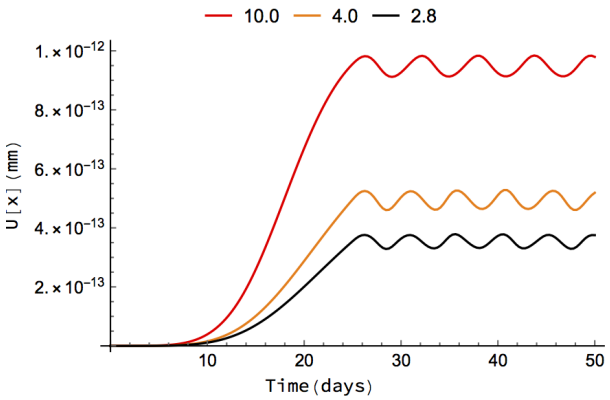

(b) Space-averaged displacement against time.

Figure 3.4: Plots showing how the displacement changes over the radius and over time, when we vary the parameter G1 (days^{-1}).

3.2 Including laminin and fibronectin

It can be seen in figures 3.2b, 3.3 and 3.4b, that the explicit numerical method applied gives solutions that are not entirely stable. This is demonstrated by the amplitude of the oscillations in the last half of the simulation. All of the results in this section have been run with an implicit numerical method which is unconditionally stable.

Figure 3.5 shows that a varying concentration of peritumoural stroma proteins affects both the magnitude of the maximum displacement, and the shape of the displacement-radius graph. However, this effect is very small, even when altering the concentration by a factor of 16. The maximum amplitude is demonstrated by the highest concentration. However, as the rate of increase in displacement over radius dips at approximately $r = 0.085$, the highest concentration also demonstrates the largest dip. It is also interesting to note that the curve representing a concentration of $1.41 \times 10^{-4}\,\mathrm{mol\,m^{-3}}$ shows the greatest disparity when compared to the other two curves, despite the factors between the three curves being equal.

The amount of displacement the tumour cells experience is no longer linear with increasing radius (within the tumour boundary). However, the shape of the displacement-radius graph outside of the tumour boundary shows much less of a difference, when compared with figures 3.2a or 3.4a.

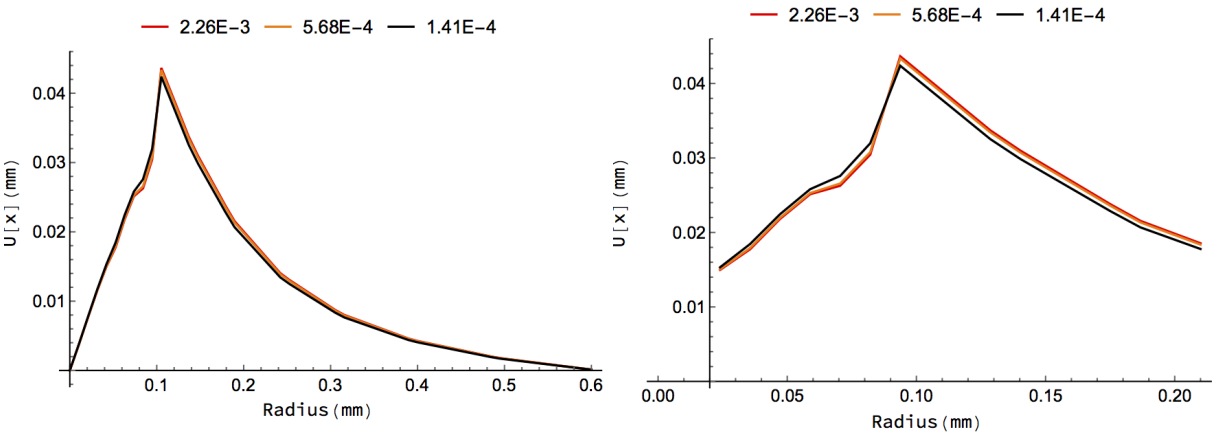

(a) Displacement against radius at 25 days.

(b) Select view from 3.5a.

Figure 3.5: Plots showing how the displacement changes over the radius when we vary the concentration of protein. Here the concentration of laminin is modelled as being constant throughout the stroma.

It can be seen from figure 3.6 that the function determining the distribution of peritumoural proteins has a large impact on both the maximum displacement within the tissue and how the amplitude of the displacement varies with increasing radius. The function with the largest effect is the simplest function, identical to that applied in figure 3.5, where the proteins have a uniform concentration throughout the stroma. It has the effect of both reducing the maximum amplitude and changing the shape of the displacement-radius graph.

Modelling the distribution of the proteins so as to be linearly increasing with radius within the tumour, and linearly decreasing outside of the tumour has almost no effect when compared with not including proteins in the model at all. However, it can just be made out in figure 3.6b that the gradient of the curve is increasing for $r < 1$. This is similarly true for the function

varying protein concentration quadratically with angle. The main purpose of implementing this quadratic concentration function was to try and simulate some isotropic growth. It cannot be seen from these figures, but it did work, though unfortunately the magnitude of this variation was so small as to be almost imperceptible.

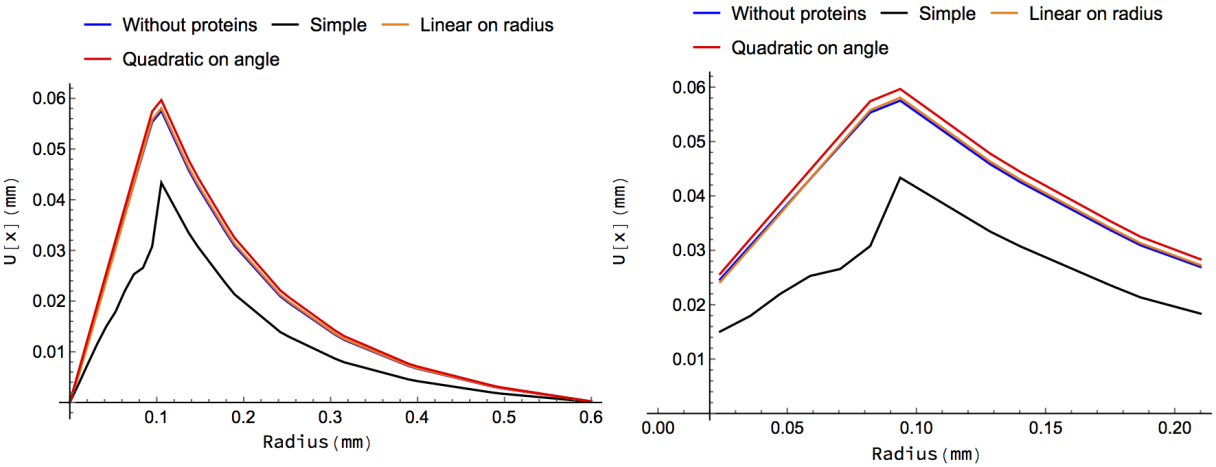

(a) Displacement against radius at 25 days.

(b) Select view from 3.6a.

Figure 3.6: Plots showing how the displacement changes over the radius when we vary the function determining the distributions of laminin and fibronectin throughout the tissue.

4 Discussion

It has been shown that decreasing the stiffness of the peritumoural stroma, increases the rate and maximum amount of tumour growth. This is as one might expect, as the tumour needs to exert less force upon a less stiff medium in order to do the same amount of work. It also makes intuitive sense that the maximum amount of displacement is seen at the tumour boundary because the growth function is only implemented for $r \leq 0.1$mm. Therefore, work is being done only for these values of r. This, in combination with the spherical symmetry of the model, means that the force exerted due to tumour growth accumulates as r increases, with the maximum force being felt at the boundary. This accumulation of force also explains why the amount of displacement increases linearly with increasing radius (until $r = 0.1$mm). The nonlinear decrease in displacement after the tumour boundary is due to the fact that the peritumoural stroma seems to be elastic in a nonlinear manner. This would also explain why the amount of stress felt decreases much more significantly than the increase in displacement, over the same change in stiffness.

It has been shown that increasing the value of G1 increases the amount of tumour growth. This is intuitive as the amplitude of the growth function $f(C)$, increases linearly with increasing G1. It also makes sense that this impact is very immediate, as our model dictates that the rate of growth is very directly link to the amplitude of the growth function, whereas dependence of the rate of growth on the stiffness of the peritumoural stroma is more convoluted.

Figures 3.2b, 3.3 and 3.4b show that the explicit numerical method gives solutions that are not entirely stable. This implies that one should use a an implicit numerical method whenever the equations allow. In section 3.1, a more complicated growth law was used. This extra complexity provided a more realistic shape to the displacement-time graphs, but increased the

computational strain, and necessitated the use of an explicit numerical method.

The magnitude of the maximum displacement increases as the concentration of peritumoural stroma proteins increases. This is what one might expect given the definition of the growth law in equation (4). It also seems consistent with our growth law definition that this effect is so small. Increasing the concentration of protein will increase the value of the quantity

$$\frac{C_{\mathrm{P}}}{G_{2,\mathrm{P}} + C_{\mathrm{P}}} \ .$$

However, this quantity will always be less than 1 for positive values of $G_{2,\mathrm{P}}$. This means that changes in the concentration will always be less significant when compared to a value of $G_{1,\mathrm{P}} = 1.4 \text{ days}^{-1}$. The effect is dampened still more when one considers that the protein concentration only affects half of the growth law, the other half being dictated by the concentration of oxygen.

It has been concluded that increasing the concentration of peritumoural proteins increases the amount of tumour growth. This means that the rate of growth when the proteins are introduced will increase. As this occurs at the tumour boundary, it will have a dampening effect on the rate of growth just inside the tumour boundary. This could explain the change of the shape of the graph shown in figure 3.5.

The function determining the concentration of protein can have an effect on both the shape and the magnitude of the displacement-radius graph. It is unclear why the simplest function (with constant stromal concentration), shows so much disparity with the other two functions. It is possible that a space-averaged magnitude would be much more similar than the maximum amplitude of the displacement.

It seems likely that the reason the other concentration functions have such a small effect on the displacement-radius curve is due to the fact that the effect of the change in protein concentration is dampened by the choice of parameters $G_{1,\mathrm{P}}$ and $G_{2,\mathrm{P}}$, as described above.

In conclusion, including the peritumoural stroma proteins laminin and fibronectin has a postive correlation on tumour growth as implemented in this model. However, the impact of this effect is dictated as much by the choice of parameters $G_{1,\mathrm{P}}$ and $G_{2,\mathrm{P}}$, as by any change in the concentration value. It seems that finding a set of values $\{G_{1,\mathrm{P}},\ G_{2,\mathrm{P}},\ C_{\mathrm{P}}\}$ is the key to the effective modelling of the inclusion of peritumoural stroma proteins.

There are several ways in which this methodology could be improved or extended. Firstly, there are other options for including the proteins laminin and fibronectin into our model. For example, we have described the contributions to the growth rate of oxygen and proteins to be combined additively in equation (4). In the work of Casciari et al. (1992a), the effect of oxygen and glucose on the growth rate are included multiplicatively. It might be appropriate to include the effect of stromal proteins multiplicatively too. The decision was made against that course here, firstly because having a multiplicative definition causes problems when the concentration of proteins is zero in that it causes the growth function $f(C)$ to be zero likewise. Equally, when comparing the effects of glucose and oxygen, the two substances have quite a similar mechanism in terms of how they affect the growth of a tumour. It has been shown by Casciari et al. (1992b) that when the concentration of oxygen is low, tumour cells compensate by increasing their uptake of glucose, and visa versa. However, the proposed mechanism for stromal proteins affecting the growth rate of a tumour is different enough that an additive model seems most appropriate.

Secondly, the theorised mechanisms for laminin and fibronectin affecting tumour growth are

biochemical. Whilst we have implemented a growth function based upon reaction kinetics, the basis of the model is biomechanical. It would be interesting to study the effects of adding peritumoural proteins with a model that relies more heavily upon biochemistry. This also raises the question of how appropriate it is to model the effect of laminin and fibronectin using a model based upon the Michaelis-Menton rate equation. It is possible that the law of mass action (Britton, 2003) could be applied to a reaction equation designed specifically for the interaction between peritumoural stroma proteins and tumour cells, and that this would increase the accuracy of our model.

Acknowledgements

I would like to thank my supervisors, Dr. Peter Wijeratne and Dr. Umber Cheema. I would also like to thank Marina Pavlou, for describing the laboratory work to me, and for providing the data in 1.3 and the photograph in figure 1.2.

A Parameter values

Sym.	Parameter Name	Value	Units	Source
μ_{T}	Shear modulus (tumour)	725	Pa	Wijeratne et al. (2015)
μ_{S}	Shear modulus (stroma)	710	Pa	Wijeratne et al. (2015)
K_{T}	Bulk modulus (tumour)	14010	Pa	Wijeratne et al. (2015)
K_{S}	Bulk modulus (stroma)	3080	Pa	Wijeratne et al. (2015)
G_1	Growth parameter 1	2.8	days^{-1}	Kim et al. (2011)
G_2	Growth Parameter 2	7.3×10^{-3}	$\mathrm{mol\,m}^{-3}$	Casciari et al. (1992b)
C_O	Concentration of oxygen	0.043	atmos. %	Casciari et al. (1992b)

Table A.1: Model parameter values used in preliminary tests

Parameter Name	Value	Units
Number of time steps	16000	(no units)
Stepsize	3.125×10^{-2}	days^{-1}

Table A.2: Numerical method parameter values used in preliminary tests

Sym.	Parameter Name	Value	Units	
μ_{T}	Shear modulus (tumour)	725	Pa	Wijeratne et al. (2015)
μ_{S}	Shear modulus (stroma)	710	Pa	Wijeratne et al. (2015)
K_{T}	Bulk modulus (tumour)	14010	Pa	Wijeratne et al. (2015)
K_{S}	Bulk modulus (stroma)	3080	Pa	Wijeratne et al. (2015)
$G_{1,\mathrm{O}}$	Growth parameter 1 (oxygen)	1.4	days^{-1}	Kim et al. (2011)
$G_{1,\mathrm{P}}$	Growth Parameter 1 (protein)	1.4	days^{-1}	This work
$G_{2,\mathrm{O}}$	Growth parameter 2 (oxygen)	7.3×10^{-3}	$\mathrm{mol\,m}^{-3}$	Casciari et al. (1992b)
$G_{2,\mathrm{P}}$	Growth Parameter 2 (protein)	5.65×10^{-5}	$\mathrm{mol\,m}^{-3}$	This work
C_{O}	Concentration of oxygen	0.043	atmos. %	Casciari et al. (1992b)
C_{lam}	Concentration of stroma protein	5.68×10^{-4}	$\mathrm{mol\,m}^{-3}$	This work

Table A.3: Model parameter values used in simulations involving laminin and fibronectin

References

Utkarsh Ayachit, Berk Geveci, and Lisa Avila. *The ParaView guide: updated for ParaView version 4.3.* Kitware, 2015.

Nicholas F. Britton. *Essential Mathematical Biology.* Springer-Verlag, 2003.

J. J. Casciari, S. V. Sotirchos, and R. M. Sutherland. Mathematical modelling of microenvironment and growth in emt6/ro multicellular tumour spheroids. *Cell Proliferation*, 25(1):1–22, 1992a.

J. J. Casciari, S. V. Sotirchos, and R. M. Sutherland. Variations in tumor cell growth rates and metabolism with oxygen concentration, glucose concentration, and extracellular ph. *Journal of Cellular Physiology*, 151(2):386–394, 1992b.

Geoffrey M. Cooper and Robert E. Hausman. *The cell: a molecular approach*. Sinauer Associates, Inc., Publishers, second edition, 2000.

Vittorio Cristini and John Lowengrub. *Multiscale Modeling of Cancer: An Integrated Experimental and Mathematical Modeling Approach*. Cambridge University Press, 2010.

Curt Deister, Samer Aljabari, and Christine E. Schmidt. Effects of collagen 1, fibronectin, laminin and hyaluronic acid concentration in multi-component gels on neurite extension. *Journal of Biomaterials Science, Polymer Edition*, 18(8):983–997, 2007.

Dennis E. Discher, Paul Janmey, and Yu-li Wang. Tissue cells feel and respond to the stiffness of their substrate. *Science*, 310(5751):1139–1143, 2005.

Jürgen Engel, Erich Odermatt, Andreas Engel, Joseph A Madri, Heinz Furthmayr, Heilwig Rohde, and Rupert Timpl. Shapes, domain organizations and flexibility of laminin and fibronectin, two multifunctional proteins of the extracellular matrix. *Journal of molecular biology*, 150(1):97–120, 1981.

Christian Frantz, Kathleen M. Stewart, and Valerie M. Weaver. The extracellular matrix at a glance. *Journal of Cell Science*, 123(24):4195–4200, 2010.

Gabriel Helmlinger, Paolo A. Netti, Hera C. Lichtenbeld, Robert J. Melder, and Rakesh K. Jain. Solid stress inhibits the growth of multicellular tumor spheroids. *Nat Biotech*, 15(8):778–783, 08 1997.

Gerhard A. Holzapfel. *Nonlinear solid mechanics: a continuum approach for engineering*. Wiley, 2000.

E Ioachim, A Charchanti, E Briasoulis, V Karavasilis, H Tsanou, D.L Arvanitis, N.J Agnantis, and N Pavlidis. Immunohistochemical expression of extracellular matrix components tenascin, fibronectin, collagen type {IV} and laminin in breast cancer: their prognostic value and role in tumour invasion and progression. *European Journal of Cancer*, 38(18):2362 – 2370, 2002.

Yangjin Kim, Magdalena A. Stolarska, and Hans G. Othmer. The role of the microenvironment in tumor growth and invasion. *Progress in Biophysics and Molecular Biology*, 106(2):353 – 379, 2011. Systems Biology and Cancer.

Anna Kane Laird. Dynamics of tumour growth. *British journal of cancer*, 18(3):490, 1964.

Michael Lieberman, Allan D. Marks, and Matthew Chansky. *Marks' basic medical biochemistry: a clinical approach*. Wolters Kluwer/Lippincott Williams Wilkins Health, third edition, 2009.

Laura Marquardt and Rebecca Kuntz Willits. Neurite growth in peg gels: effect of mechanical stiffness and laminin concentration. *J Biomed Mater Res A*, 98(1):1–6, 2011.

Agata Nyga, Umber Cheema, and Marilena Loizidou. 3d tumour models: novel in vitro approaches to cancer studies. *Journal of Cell Communication and Signaling*, 5(3):239, 2011.

Agata Nyga, Marilena Loizidou, Mark Emberton, and Umber Cheema. A novel tissue engineered three-dimensional in vitro colorectal cancer model. *Acta Biomaterialia*, 9(8):7917 – 7926, 2013.

Vasileios Vavourakis and Peter Wijeratne. Feb3 (finite element bioengineering in 3d). URL: `https://bitbucket.org/vasvav/feb3-finite-element-bioengineering-in-3d/wiki/Home`, 2016. [Accessed 5-February-2017].

C. Voutouri, F. Mpekris, P. Papageorgis, A. D. Odysseos, and T. Stylianopoulos. Role of constitutive behavior and tumor-host mechanical interactions in the state of stress and growth of solid tumors. *PLoS ONE*, 9(8), 2014.

Peter A. Wijeratne, Vasileios Vavourakis, John H. Hipwell, Chrysovalantis Voutouri, Panagiotis Papageorgis, Triantafyllos Stylianopoulos, Andrew Evans, and David J. Hawkes. Multiscale modelling of solid tumour growth: the effect of collagen micromechanics. *Biomechanics and Modeling in Mechanobiology*, 15(5):1079–1090, 2015.